MEMS Implementation in Altitude Stabilization for Unmanned Vertical Take-off/Landing Aircraft

[1] Thanakorn Supsukbaworn, [1,]* Chin E. Lin and [2] Hsin-Yuan Chen

Abstract

Abstract— Unmanned vertical take-off/Landing (UVTOL) Aircraft have received great attention for their flexibility and controllability in many applications requiring short range, low altitude air surveillance. Image acquisition and video recording from the air is useful for many demands. The operation of a UVTOL requires altitude stabilization with a very limited payload. This paper presents a flight control stabilization design using a MEMS (microelectronics mechanical system) inertial sensor and a barometric sensor to enhance the altitude stabilization performance. By introducing pressure, velocity, and acceleration estimators, a modified flight controller is constructed and tested. Altitude and vertical velocity stabilization are tested and verified using real flight data.

Keywords: UVTOL Aircraft, Data Estimator and Filter, MEMS sensor, Flight Tests, Altitude Control.

1. Introduction

Unmanned Aircraft System (UAS) or Remote Piloted Vehicle System (RAPS) have been widely used in civilian applications. In disaster rescue missions, Unmanned Aerial Vehicles (UAVs) engage in surveillance in advance before manned system is deployed. UAV collects and sends surveillance data to rescue team in data and video via communication. UAVs obviate the risk of using human pilots in unknown and potentially dangerous airspace [1]. Recently, the unmanned vertical take-off and landing (UVTOL) vehicles have been developed for various applications. UVTOLs can be launched and operated near the emergency site for more rapid data acquisition and report. Although the operation of UVTOLs is supported by the public, some important factors relating to demand, risk, cost and maneuverability [2] must be carefully considered either in development or in deployment.

*Corresponding Author: Chin E. Lin
(E-mail: chinelin@mail.ncku.edu.tw)
[1]Department of Aeronautics and Astronautics, National Cheng Kung University, Tainan, Taiwan
[2]Department of Computer Science and Information Engineering, National Chun-Yi University of Technology, Taichung, Taiwan*

When an accident happens, ground obstructions, debris, injuries and victims may cause difficulties in search and rescue. Accident site surveillance may thus be especially important. For example, in the Asiana Flight 214 accident on July 6, 2013, one victim was severely injured by the rescue team itself, due to the lack of information about the scene [3]. A rapid survey before the rescue mission may reduce the risk of misidentifying scattered objects on the ground and increase the efficiency of the rescue effort. UAVs may also provide information that facilitates direct rescue of victims.

Risk of operation to human beings is always the main concern when UAVs are flown in close proximity to inhabited areas. Disaster sites may include fires and unpredictable surfaces, as well as humans moving around. A safe and reliable flying platform should be considered from the beginning of the system design [4]. Since the ground surface is always rough and unpredictable at the accident site, ultrasonic devices may not correctly locate ground level. Thus, a high precision low altitude vertical navigation controller is required to prevent accidents.

The UAV operating cost is a key parameter in determining the feasibility of civil UAV systems, which must be maintainable and operable at low cost. Currently, the total cost for modern civil UAS may exceed that of manned aircraft. However, the development of motor driving technologies using sensors and electronics has become more widespread and mature. MEMS (microelectronics mechanical system) inertial sensors and electrical flight systems can greatly reduce the cost and size of the aircraft. However, the accuracy and reliability of these systems must be improved.

Given the demand for low cost, accurate flight systems for UAVs, this paper focuses on the design of altitude and vertical velocity estimation for UVTOLs using MEMS accelerometers, gyroscopes, and piezo-resistive pressure transducers. System design and implementation is described and data from actual flight tests is collected. Under vertical stability flight control, the UVTOL in this can record good quality video and images. Such imagery will be useful in disaster evaluation and response.

2. Altitude Controller Design

The altitude performance of a UVTOL aircraft is influenced by its overall weight. A system with high inertia and a simple but robust PID controller is capable of achieving flight stability [5]. However, its mission may require the aircraft to acquire imagery from both high and low altitudes. A velocity controller is thus necessary to prevent the system from overshooting its intended altitude when ascending or descending, since an overshoot on descent may lead to a crash. A velocity controller allows more aggressive performance to improve system operation while limiting overshooting. A simplified model of the proposed VTOL altitude controller is shown in Figure 1.
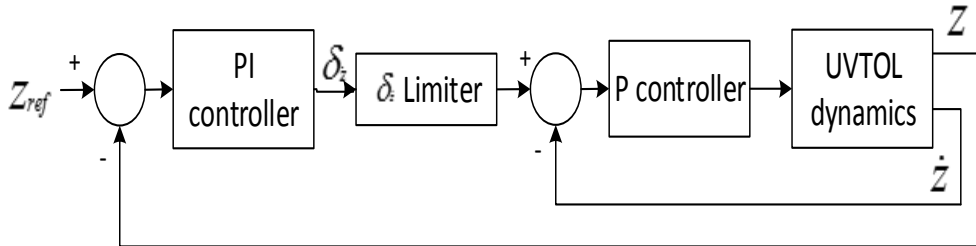

Figure 1: Simplified model of the proposed VTOL altitude controller.

In the first step, a PI roll controller responds to the altitude command Z_{ref}. The PI controller is added to compensate for any uncertainty or residual error in control such as a battery voltage change or a sudden gust of wind. The second stage is designed for vertical velocity control where the rate of change of the airframe in height $\delta_{\dot{z}}$ is limited. This stage of the controller is designed to rapidly respond to the rate of change of the airframe to improve the stability of the altitude. Using the $\delta_{\dot{z}}$ limiter, an aggressive response to the inner loop can be maintained while overshoot is minimized.

3. Filter Design

3.1 Altitude Filter Design

A piezo-resistive pressure sensor is used as an altimeter that measures change in height. The pressure as measured in Pascal is converted to a change in height in meters by [6]:

$$\Delta h = 4330 \cdot \left(1 - \left(\frac{P}{P_0}\right)^{0.19}\right) - h_{init} \qquad (1)$$

where h_{init} is calculated at P_{init} and P_0 is the standard pressure defined as 101.325kPa. The height measurement contains noise and drift due to ambient temperature and pressure fluctuation. The amplitude of fluctuation varies with weather, wind speed, and season [7].
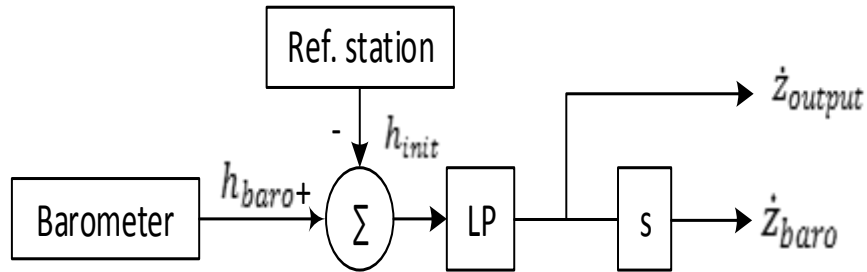

Figure 2: Altitude estimator signal flow diagram.

From Figure 2, the change in h_{init} on the ground can be measured by the ground station. Thus, the ambient fluctuation can be suppressed. In this paper, one reference barometer on the ground is used as the reference station. Δh is sensed from the reference station and sent with altitude reading drift to the platform. The data output of the pressure sensors at 200Hz sampling rate has a standard deviation of about 5.8cm with a noise amplitude of ±15cm after being converted into altitude. The data is then passed through the low-pass filter. The formula for the low-pass filter for this operation is:

$$x_n = \propto x_s + (1-\propto)x_{n-1} \qquad (2)$$

where x_n and x_{n-1} are the current and previous value of the state, respectively. x_s is the new sample of the filter or the filter input.

After passing through the low-pass filter, Z_{output} represents the altitude for control system while $\dot{Z}_{baro}$ is the estimated vertical velocity from the barometer.

3.2 Vertical Velocity Filter Design

Ideally, to estimate the change in height, the differentiation term from barometric altitude data can be adopted and passed to the controller directly. In reality, differentiation to the noisy data amplifies the noise, especially at the high sampling rate of 200Hz. The direct use of differentiated data may trigger

unstable performance by the control system [8].

The velocity of the airframe can be collected from the accelerometer. A three-axis miniature MEMS accelerometer is adopted to provide the direction of the acceleration vector. Unfortunately, the MEMS sensor is subject to thermal bias, white noise, offset, and change due to environment [9]. Those errors are small when compared to their magnitude. But by integration through time, those errors will result in a significant effect on velocity.

A MEMS rate gyroscope is added to determine the angular rate of the airframe. Using the sensor fusion algorithm, the low cost gyroscope and accelerometer can provide attitude information for roll and pitch [10]. However, the attitude estimation using these sensors contains errors which may vary within a range of a few degrees. Using the attitude information and data from accelerometer, the acceleration in the inertial frame can be obtained by:

$$\vec{a}_I = C_B^I \vec{a}_m - \begin{pmatrix} 0 \\ 0 \\ g \end{pmatrix} \qquad (3)$$

where a_m refers to measured acceleration from the accelerometers, a_I refers to acceleration in the inertial frame with gravity subtracted, g is gravity defined as $9.81 m/s^2$, and C_B^I is the rotation matrix from the body frame to the inertia frame, defined as:

$$C_B^I(\emptyset,\theta,\varphi) = \begin{pmatrix} c(\varphi)c(\theta) & c(\varphi)s(\emptyset)c(\theta)-c(\emptyset)s(\varphi) & s(\emptyset)s(\varphi)+c(\emptyset)c(\varphi)s(\theta) \\ c(\theta)s(\varphi) & c(\emptyset)c(\varphi)+s(\varphi)s(\emptyset)s(\emptyset) & c(\emptyset)s(\varphi)s(\emptyset)-s(\emptyset)c(\varphi) \\ -s(\theta) & c(\theta)s(\emptyset) & c(\emptyset)c(\theta) \end{pmatrix} \qquad (4)$$

where the letter s represents sin and the letter c represents cos, respectively.

In practice, data is obtained regularly at discrete time intervals. The estimated velocity may further be obtained by integration of acceleration using:

$$\dot{z}_{accel}[k+1] = \dot{z}_{accel}[k] + T(a_z[k] - \ddot{z}_{offset}) \qquad (5)$$

where T is the sampling period at 200Hz in this study, a_z is acceleration in the z axis, $\ddot{z}_{offset}$ is the bias of accelerometer reading which has to be cancelled, $\dot{z}_{accel}$ is the estimated velocity obtained from accelerometer. The overall process in obtaining $\dot{z}_{accel}$ is illustrated in Figure 3.
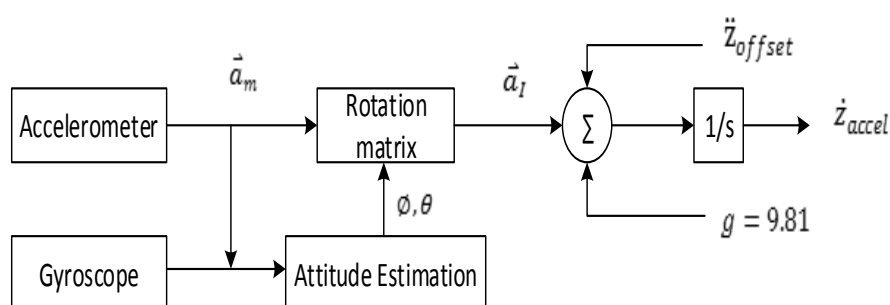

Figure 3: $\dot{z}_{accel}$ **estimator signal flow diagram.**

Offset of accelerometer can be calculated from monitoring rate of error calculated from $\dot{z}_{accel}$ and $\dot{z}_{baro}$. Although $\dot{z}_{baro}$ is very noisy since it is obtained from differentiation of barometer output. However, its long term stability is better than $\dot{z}_{accel}$. The $\ddot{z}_{offset}$ cancellation method is applied to stop growing error in $\dot{z}_{accel}$. Furthermore, the error in $\dot{z}_{accel}$ that has already accumulated before the cancellation response, must also be eliminated. The offset estimation process is described in Figure 4.
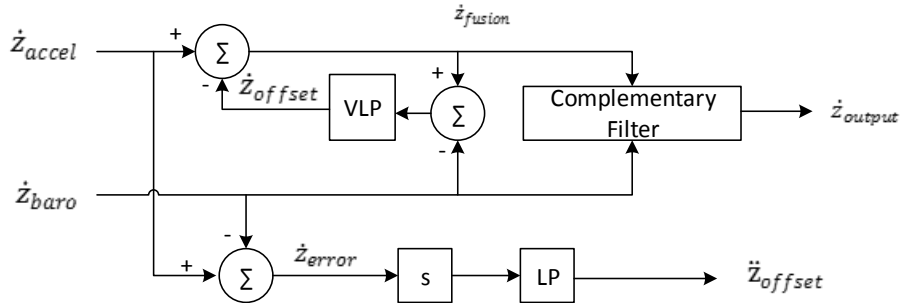

Figure 4: Offsets estimator signal flow diagram.

The bottom section of Figure 4 shows the $\ddot{z}_{offset}$ estimator algorithm. The difference between the speed estimator by the barometer and accelerometer is estimated in each update. The rate-of-change of error is then monitored by differentiating between each reading. Since the data after differentiation is noisy, it is necessary to filter the $\dot{z}_{error}$ using a low-pass filter with a very low cutoff frequency.

The upper loop of Figure 4 shows the $\dot{z}_{offset}$ tracking loop. Since the $\ddot{z}_{offset}$ may contain a time delay that affects the response or the numerical integration error of $\dot{z}_{accel}$ estimator, so it's necessary to have another loop to minimize the error that has been integrated into signal. $\dot{z}_{offset}$ is a parameter that keeps tracking the error $\dot{z}_{accel}$ before it is complemented with $\dot{z}_{baro}$. It is noted that the $\ddot{z}_{offset}$ tracking loop and $\dot{z}_{offset}$ has to be estimated in two different loops. Otherwise, they may have a coupled response due to cross correction between the two loops. Finally, the complementary filter between $\dot{z}_{baro}$ and $\dot{z}_{fusion}$ is applied to compensate for the slow response of the offset tracking loop. The complementary filter allows the offset tracking loop to work accurately while responding rapidly when a reading error remains. The complementary filter may be expressed as:

$$\dot{z}_{output} = k_c \cdot \dot{z}_{baro} + (1 - k_c) \cdot \dot{z}_{fusion} \quad (6)$$

where $0 \leq k_c \leq 1$

4. Implementtion for VTOL Altitude Stabilization

The microcontroller based hardware for implementation is shown in Figure 5. A 16 bit dsPIC30F6010A microcontroller from Microchip is used as the signal processing unit. The miniature MEMS gyroscope and accelerometer are connected to the microcontroller unit via an I2C bus at a sampling rate of 200Hz. The piezo-resistive analog pressure sensor MPX6115A signal is sampled using an analog-to-digital converter ADS1246 which has a sampling frequency of 200Hz. The ADC is controlled to communicate with the microcontroller via the SPI bus. The reference station is set on the ground and transmits the deviation in reading height to the moving unit via an XBee wireless modem. The data output is connected to a computer via an RS-232 port for monitoring and analysis.
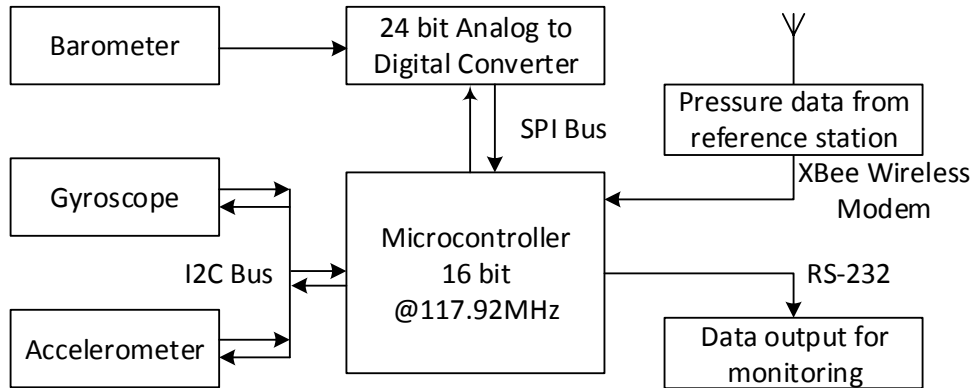
Figure 5: Hardware schematic for the current experiment.

The first experiment is taken to examine the precision and accuracy of the barometric height estimated with and without correction from the reference station. The sensor unit and reference unit are installed statically at a distance of about 10 meters. The data was captured is initiated at from 5 a.m. to noon on a calm day to evaluate the difference in the atmospheric changes.

The second experiment studies the accuracy and performance of the velocity estimation algorithm. The sensor module was hand carried into an elevator by one of the researchers. It was thus affected by the uncertainty of attitude as the hand shifted its position. The elevator was commanded to go up and down from 1st floor to 12nd floor. Note that the reference station is not connected to the signal processing unit at this time because it is not possible to transmit a wireless signal into the elevator and the pressure deviation in such a short period of time is expected to be small.

5. Experiments

5.1 Reference Station Effect in Offset Cancellation Result

The altitude data for the 7 hours is shown in Figure 6. Figure 6(a) shows the correlation between the movement of the altitude data between the reference station and the sensor unit. At its greatest, the deviation was 20 meters in 5 hours. The highest rate of error is at the time from 5 a.m. to 6 a.m., about daybreak, where there can be more than 10 meters of change per hour.

Figure 6(b), shows the results after receiving the reference station data. The deviation is relatively small in the morning (i.e. ± 0.2 m). However, after sunrise, the deviation and fluctuation appears to grow larger. The deviation can be as high as ± 1 m for short periods of time. The trend in the residual error shows that the fluctuation is greater than the propagation of the pressure. However, the error of ± 1 m is considered satisfactory and safe.
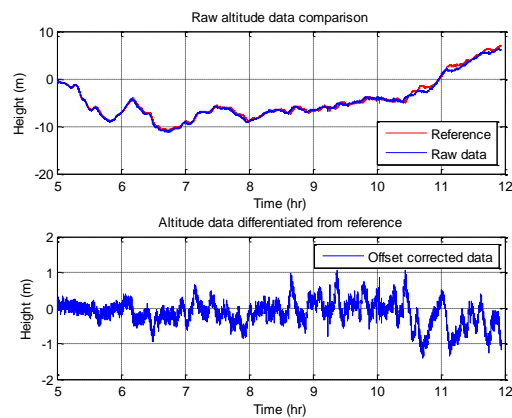

Figure 6: (a) raw altitude data (top), (b) altitude data with reference station input (bottom)

This experiment shows the necessity of using the reference barometer data for correction. Since UVTOLs have an endurance of about an hour, the use of uncorrected barometers in a low-altitude mission may lead to an error of 10 meters. This is unacceptable in an area where safety is the most important consideration.

5.2 Vertrical Velocity Estimation Result

A dynamic test was performed on the system hardware without the reference station. The result of vertical velocity estimation $\dot{z}_{output}$ is shown in Figure 7.
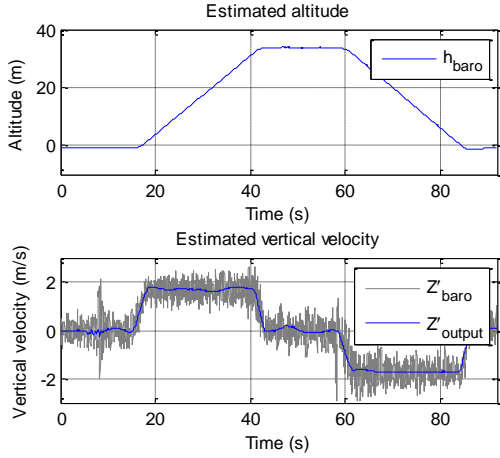
Figure 7: (a) barometer altitude data (top), (b) estimated vertical velocity compared to the barometer data (bottom)

Figure 7(a) shows the altitude estimated without using the reference station. The estimated height of the 1st floor is -0.7 meter from the initial point, while for the 12th floor it is 51 meters. The slope of the curve is steady, indicating the constant velocity during the journey. At the end of the capture, around the 90th second, the estimated height is about -0.93 meters from the initial point.

Figure 7(b) shows the estimated velocity from the device. $\dot{z}_{baro}$ appears to be noisy and sensitive to movement. Instead, the $\dot{z}_{output}$ shows the smooth output without delay. The maximum velocity measured during ascending and descending was $1.7 \pm 0.1\,\text{m/s}$ and $1.65 \pm 0.1\,\text{m/s}$, respectively.

5.3 Real-time Offset Tracking Eesult

The performance of $\dot{z}_{offset}$ in the offset tracking loop is shown in Figure 8(a). The data from the 20th second to the 40th second show that $\dot{z}_{accel}$ drifts away from the location where it is supposed to be. $\dot{z}_{offset}$ at the 40th second is about $-0.4\,\text{m/s}$. The drift is due to an acceleration error which grows constantly. However, the tracking loop has detected this error and cancelled it. Figure 8(b) shows the response due to the acceleration error. The initial value of $-0.064\,\text{m/s}^2$ is obtained from initialization. Because the interior and exterior of the elevator have different environments, the offset has changed but is still within the performance of the $\ddot{z}_{offset}$ tracking loop. However, because the filter tuning is imperfect, the response of the tracking loop still suffers from the change in the barometer. Note that this experiment is done during the day time when the fluctuation in pressure is high. However, the convergence of the filter and successful offset cancellation make this result acceptable.
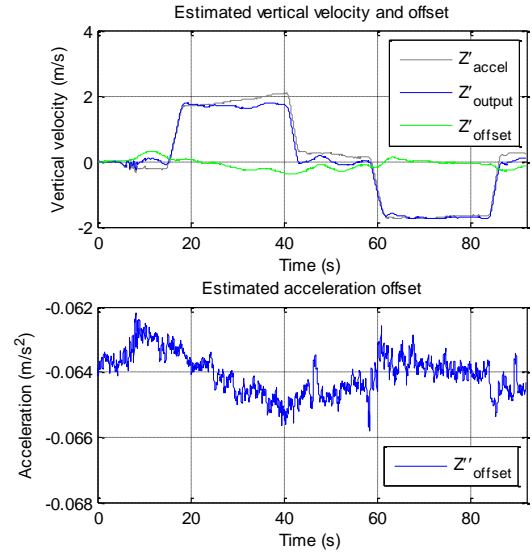

Figure 8: (a) $\dot{z}_{offset}$ tracking loop performance (top), (b) $\ddot{z}_{offset}$ tracking loop performance (bottom)

5.4 Close-loop Response Performance Experiments

In order to understand the performance of the proposed control algorithm, the implementation and flight tests were conducted on a $35\,\text{cm} \times 35\,\text{cm}$ size quad-rotor, as shown in Figure 9. The filtered altitude and vertical velocity data were fed through the proposed altitude control algorithm. The quad-rotor was first commanded to hold the altitude, prior to actual flight. After that, 2 meters step input in altitude was sent to the flight control. The vertical velocity limit boundary for the airframe was set to $1.0\,\text{m/s}$. The experimental flight data results are recorded.

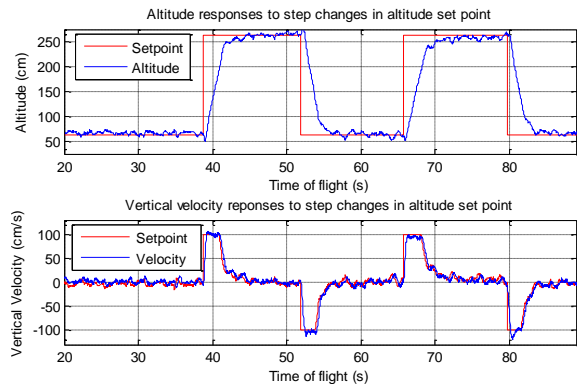**Figure 9: The experimental quad-rotor UAV.**

Figure 10: (a) Altitude close loop performance (top), (b) Vertical velocity close loop performance (bottom)

Figure 10a shows the altitude response to the given set point. From the 20th to 38th second, the altitude holding performance was stable as the deviation in altitude control was about ±15cm. At the 39th, 52nd, 66th and 68th second, where the step inputs were given, the aircraft rose and fell at a constant rate at the beginning and slowed when it came closer the set point. The stable climb and descent is a result of inner-loop velocity control. Average settling time for step inputs was 4.3 seconds.

Figure 10b verifies the performance of the velocity control. As the step inputs were given, the airframe rose or descended at a maximum allowable speed of ±1.0m/s, which then fell slowly as the altitude error became smaller. Average settling time for all four step inputs was 0.7s. Average deviation in vertical velocity during the altitude holding section is about ±10cm/s.

The velocity limiting appeared to improve the flight performance and flight stability. If the allowable speed is not controlled, the sudden rise in the throttle command to motors may lead to an abrupt change the power consumption if the velocity error is large. The sudden increase in power consumption may also lead to a voltage drop in the power loop and result in temporary loss of other stabilization functions.

By using the proposed filter and control algorithm, the flight control system can control the airframe within a high degree of precision, ±15cm, allowing the velocity to be controlled with an accuracy level of ±10cm/s. With the reference station, the long-term accuracy can be ±1.2m which is suitable for outdoor disaster rescue missions where smooth and precise control is required.

Furthermore, the closed loop control response system is tested under external disturbance. This condition is simulated by manually pushing/pulling the airframe to force the UVTOL to deviate from the altitude set point, as shown in Figure 11. Shaded areas mark the approximate period where the external force is applied. For the first applied deviation in altitude, the UVTOL was pushed up 86cm from the

set point. It recovered to ±15cm from the set point in 0.78 second after release from the external force. The second disturbance was pulling the UVTOL down by 72cm from the set point. Note that the person who was giving the push experienced a strong resistance response from the aircraft in this action. It recovered to ±15cm from the set point in 0.96 second after release from pulling. No unstable behavior was experienced after the response was finished. The altitude stabilization test using a simulated external disturbance appears to be satisfactory.
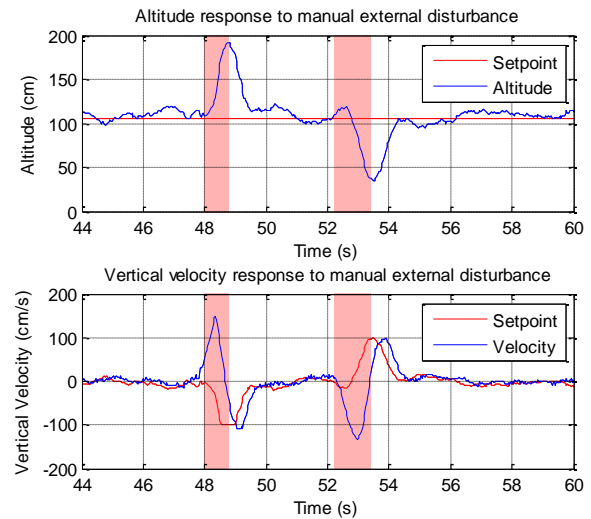

Figure 11: (a) Altitude response to external disturbance (top), (b) Vertical velocity response to external disturbance (bottom)

6. Conclusion

The altitude and vertical velocity estimation for UVTOL using low cost light-weight miniature sensors to determine and eliminate errors is verified with a satisfactory performance under actual test conditions. The output altitude with a reference station can maintain the accuracy within a 1 meter bound despite the daily atmospheric pressure fluctuation. Flight test results also enable understanding of the high precision of altitude control performance with estimated data. The vertical velocity estimation loop returns an accurate value with stable output which is suitable for further implementation into the altitude controllers of UVTOLs for on-site surveillance applications. Given the excellent vertical stability, the image capture quality may potentially be improved. Since the estimation algorithm is based on low cost miniature devices, this stabilization design may also be used in other applications.

Acknowledgment

References

[1]. S. M. Adams, C. Friedland, "A Survey of Unmanned Aerial Vehicle (UAV) Usage for Imagery Collection in Disaster Research and Management," 9th International Workshop on Remote Sensing for Disaster Response, September 2011.

[2]. W. M. DeBusk, "Unmanned Aerial Vehicle Systems for Disaster Relief: Tornado Alley," AIAA Infotech@Aerospace Conference, AIAA-2010-3506, Atlanta, GA, April 20-22, 2010.

[3]. M. Michael, "Attorney: Asiana crash video shows firefighters didn't help girl soon enough", CNN (Jan. 16 2014).

[4]. K. K. Bhamidipati, D. Uhlig, N. Neogi, "Safety and Reliability into UAV Systems: Mitigating the Ground Impact Hazard", AIAA Guidance, Navigation and Control Conference and Exhibit, August 2007.

[5]. Y. Luo, L. Di, J. Han, H. Chao, Y. Chen, "VTOL UAV altitude flight control using fractional order controllers," Proc. of the 4th IFAC Workshop on Fractional Differentiation and Its Application, Badajoz, Spain, October, 18-20, 2010.

[6]. M. Tanigawa, H. Luinge, L. Schipper, P. Slycke, "Drift-free dynamic height sensor using MEMS IMU aided by MEMS pressure sensor," Proc. of 5th Workshop on Positioning, Navigation and Communication, 2008, Hannover, Germany, March 2008, pp. 191-196.

[7]. H. Richner, "Pressure fluctuations caused by atmospheric waves and their variation under different weather conditions," Arch Meteorol Geophys Bioklimatol, A Meteorol Geophys, 26:309–22 1977.

[8]. G. C. Goodwin, S. F. Graebe, M.E. Salgado, Control System Design, New Jersey: Prentice Hall, 2001.

[9]. Pang, G.; Liu, H.; "Evaluation of a Low cost MEMS Accelerometer for Distance Measurement", Journal of Intelligent and Robotic System, Vol. 30, 2001, pp. 249 - 265.

[10]. Y.C. Lai, S.S. Jan, F.B. Hsiao, "Development of a low cost attitude and heading reference system using a three-axis rotating platform," Sensors, Vol. 10, No. 4, 2010, pp. 2472–2491.

Thanakorn Supsukbaworn was born in Bangkok, Thailand. He Received BS from Department of Aerospace Engineering, Kasetsart University, Thailand in 2012. He has attended Master Program and then in Ph. D. Program in Department of Aeronautics and Astronautics, National Cheng Kung University, Tainan, Taiwan since 2012. His research interests are control system design and implementation, unmanned aerial vehicle, MEMS and Microcontroller design in control applications.

Chin E. Lin was born in Chang Hua, Taiwan. He received BSEE and MSEE from Department of Electrical Engineering, National Cheng Kung University, Tainan, Taiwan, in 1975 and 1977, respectively. He received Doctor of Engineering from Department of Electrical Engineering, Lamar University, Beaumont, Texas in 1983. Dr. Lin is currently Professor in Department of Aeronautics and Astronautics, National Cheng Kung University. His research interests are control applications, avionics system, wireless data surveillance system, magnetic suspension system, and e-commerce system.

Hsin-Yuan Chen was born in Taichung, Taiwan. She received the B.S., the M.S. and Ph.D. degrees in Aeronautical and Astronautical Engineering from the National Cheng Kung University (NCKU), Tainan, Taiwan in 1994, 1996 and 2000, respectively. She received the Ph.D. degree in Electrical Engineering from the UCLA, U.S., 2011. She had been with Feng Chia University (FCU), Taichung, Taiwan, where she was the Professor of Automatic Control Engineering Department from 2000-2010. Currently, she is an adjunct professor in the Department of Computer Science and Information Engineering, National Chun-Yi University of Technology, Taichung, Taiwan. Her current research interests are Artificial Intelligence, Internet of Things, robust control, Navigation systems, neural networks, fuzzy systems, fuzzy neural networks, and intelligent wireless Systems.